Hybrid lead halide perovskites for ultrasensitive photoactive switching in terahertz metamaterial devices

Manjappa, Manukumara; Srivastava, Yogesh Kumar; Solanki, Ankur; Kumar, Abhishek; Sum, Tze Chien; Singh, Ranjan

2017

Manjappa, M., Srivastava, Y. K., Solanki, K., Kumar, A., Sum, T. C., & Singh, R. (2017). Hybrid lead halide perovskites for ultrasensitive photoactive switching in terahertz metamaterial devices. Advanced materials, 29(32), 1605881-. doi:10.1002/adma.201605881

https://hdl.handle.net/10356/138740

https://doi.org/10.1002/adma.201605881

Hybrid Lead Halide Perovskites for Ultrasensitive Photo-Active Switching in Terahertz Metamaterial Devices

Manukumara Manjappa,[1,2] Yogesh Kumar Srivastava,[1,2] Ankur Solanki,[1] Abhishek Kumar,[1,2] Tze Chien Sum,[1] and Ranjan Singh[1,2,]*

[1]Division of Physics and Applied Physics, School of Physical and Mathematical Sciences, Nanyang Technological University, 21 Nanyang Link, Singapore 637371, Singapore

[2]Centre for Disruptive Photonic Technologies, The Photonics Institute, 50 Nanyang Avenue, Nanyang Technological University, Singapore 639798

* Corresponding author: ranjans@ntu.edu.sg.

Keywords: organic-inorganic metal halide perovskites, Fano resonance, ultrafast switching, active photonics, metamaterial-phonon coupling

Abstract:

The recent meteoric rise in the field of photovoltaics with the discovery of highly efficient solar cell devices has been inspired by solution-processed organic-inorganic lead halide perovskites that exhibit unprecedented light to electricity conversion efficiencies. The stunning performance of perovskites is attributed to its strong *photo responsive* properties that has been thoroughly utilized in designing excellent perovskite solar cells, light emitting diodes, infrared lasers, and ultrafast photodetectors. However, optoelectronic application of halide perovskites in realizing highly efficient subwavelength photonic devices has remained a challenge. Here, we exploit the remarkable photoconductivity of the organic-inorganic lead halide perovskites to demonstrate a hybrid perovskite-metamaterial device that shows extremely low power photo-switching of the metamaterial resonances in the terahertz part of the electromagnetic spectrum. Furthermore, we observed a signature of a coupled phonon-metamaterial resonance at higher pump powers, where the Fano resonance amplitude is extremely weak. In addition, we also observed a low threshold, dynamic control of the highly confined electric field intensity in the system that could tremendously benefit the new generation of subwavelength meta-photonic devices as active sensors, low threshold optically controlled lasers and active nonlinear devices with enhanced functionalities in the infrared, optical and the terahertz parts of the electromagnetic spectrum.

Introduction

The recent advances in the solution-processed organic-inorganic metal halide perovskite semiconductors have triggered tremendous opportunities in the field of photonics[1,2] and solar cell technologies.[3,4] Steep rise in the power conversion efficiencies of these optoelectronic devices in the recent years has enhanced their performance as the clean energy sources, light emitting devices[5,6] and semiconductor amplifiers.[7,8] Unlike the silicon based photovoltaic devices, perovskites have shown high charge-carrier mobility (greater than 20 cm^2 V^{-1} s^{-1})[9], longer diffusion lengths (in the range of micrometers)[10,11] and higher efficiencies[12,13] that have led to rapid advances in the solution-based photovoltaic devices. Perovskites are of the structural form AMX_3, where A is the organic cation (CH_3NH_3), M is the metal cation and X (= Cl, Br, I) is the halide anion. Lead metal based organic-inorganic $CH_3NH_3PbI_3$ perovskite is an extensively studied perovskite that has shown exceptional power conversion efficiencies up to 20%.[14] Recently, these solution-processed perovskite films have shown low threshold optical gain and lasing characteristics with broadband tunability from visible to infrared frequencies.[2,7,15,16] Although the promising device features of solution-processed perovskite as an efficient solar cell material has been extensively studied, their potential as active photonic devices at terahertz frequencies of the electromagnetic spectrum remains unexplored. Terahertz time domain spectroscopy offers a useful tool to investigate the complex optical constants of semiconductor materials due to its non-invasive techniques without the need of Kramers-Kronig transformation. Recently, optical pump and terahertz probe measurements revealed the charge carrier dynamics in the perovskite sample and reported larger mobility and higher diffusion lengths.[17-19] Low temperature measurements at terahertz spectrum have also revealed the structural phase transition of the perovskite samples from tetragonal to orthorhombic at 165 K, where the higher order processes such as Auger recombination become dominant.[20,21] With these remarkable multifunctional properties, perovskites offer the trending research and their properties can be enhanced or exploited as an efficient photonic device by integrating them with the subwavelength resonant structures such as electromagnetic metamaterials.[22]

Metamaterials[23] offer unique prospects for the manipulation of incident light and have demonstrated novel phenomena like negative refraction[24], super-lens[25], and artificial magnetism[26]. Active control of metamaterial resonances is extremely important for realizing metadevices that could have real time control and practical applications. In the past, standard optoelectronic materials such as silicon on sapphire (SoS) and gallium arsenide (GaAs) have

been used as photo-active materials[27-29] to tune the terahertz metamaterial resonances. More recently, reconfigurable metamaterials[30,31] and graphene[32] based active devices have been demonstrated at terahertz frequencies. In this work, we demonstrate an active, high speed and ultrasensitive modulation of the Fano resonances in a metamaterial using the photo-induced conductivity change of the solution processed perovskite thin film spin-coated on a planar metamaterial structure. Spin-coating the metamaterials with solution-processed perovskites offers unprecedented advantages over the current state-of-the-art materials [27-29] used in the fabrication of active terahertz metamaterials in terms of the cost and simplification in the clean room processing steps. It is economical and extremely easy process to integrate the solution-processed perovskite material on top of the metamaterial surface. Here, we also show that the solution processed perovskite possessing substantial lattice/surface defects can act as an efficient photo-active material at terahertz frequencies compared with the defect free, epitaxial grown, lattice matched substrate such as SoS. Moreover, the astonishing photo-conductivity and optical properties of the perovskites can be blended with unnatural properties of metamaterial resonances to realize new generation of active subwavelength photonic metamaterial devices[22] together with new possibilities of probing the resonant and non-resonant interactions within the hybrid perovskite-metamaterial system. The present work is an experimental demonstration of lead halide perovskite based active control of Fano resonances in a hybrid perovskite-metamaterial system, wherein the photo-excitation of perovskite layer spin coated on the metamaterial structure actively modulates and switches-off the Fano resonance feature in the terahertz asymmetric split ring (TASR) resonator structure. It also shows a signature of phonon-metamaterial resonance coupling in the form of a mode splitting of the resonance feature at higher pump fluences. As Fano resonances in metamaterials [33,34] offer a strong confinement of the electric fields, such Fano-perovskite hybrid system can aid in enhancing the energy conversion efficiencies and could play a significant role in realizing the lasing spaser[35] with enhanced optical gain, ultrasensitive sensors and nonlinear applications.

Fabrication Process of Perovskite-Metamaterial hybrid device

The device architecture is revealed in Fig. 1(a), which describes the schematic of perovskite coated TASR metamaterial structure along with the unit cell dimensions shown in the inset of the figure. The TASR metamaterial sample was fabricated using the conventional photolithography technique, where 200 nm thick aluminum structures were deposited on a 1

mm thick z-cut quartz substrate as shown by the optical microscope image in Fig. 1(b). A 60 nm thin perovskite film was spin-coated on the TASR metamaterial sample with a good uniformity (see optical microscope image in Fig. 1(c)). A standard method based on magnetic stirring[36] was used to prepare the perovskite ($CH_3NH_3PbI_3$) sample and the preparation process is detailed in the Supporting Information. To extract the terahertz optical properties of the solution-processed perovskite material, we optically characterized a 60 nm thin layer of $CH_3NH_3PbI_3$ perovskite film deposited on a 1 mm thick z-cut quartz substrate using the transient terahertz spectroscopy. Thickness of the spun-coated perovskite layer was determined by the surface profilometry measurements and is shown in the provided Supporting Information.

Results and Discussion

Optical characterization of the perovskite spun-coated TASR metamaterial sample was performed using the Optical-pump-Terahertz-probe (OPTP) measurements in a ZnTe nonlinear crystal based THz-TDS system (details are provided in the Supporting Information). The recorded terahertz transmission spectra are shown in Fig. 2(a), for varying pump fluences of the optical excitation pulse. The strong resonance feature shown by the black curve in Fig. 2(a) represents the experimentally measured transmission spectrum for a planar TASR metamaterial structure with an asymmetry of x = 15 μm, without the spin-coated perovskite layer. It exhibits a strong Fano line-shaped resonance feature at 0.75 THz possessing a quality factor (Q) of 6.3 and broad dipolar resonance at 1.09 THz having a Q-factor of 3. The observed Fano resonance feature is due to destructive interference between the super-radiant dipole mode of the metamaterial and the weak sub-radiant mode that arise from the asymmetry in the structure.[33,34] Once the halide perovskite layer is uniformly spin-coated on the metamaterial sample, we witness a reduction in the amplitude and red shift of the Fano resonance frequency, as shown by the red curve in Fig. 2(a). This change is due to the screening of fringing fields in the TASR-structure by the semiconducting perovskite layer. This screening effect drastically decreases the capacitance at the split gaps of the Fano resonators throughout the metamaterial lattice, which results in the reduced strength of Fano resonance. Once the optical pump beam of fluence = 3.5 μJ/cm^2 (power = 1 mW) photo-excites the perovskite-TASR metamaterial hybrid sample, a strong reduction in the amplitude of the Fano resonance is observed. For 10.5 μJ/cm^2 (3 mW) of pump fluence (power), there is further reduction in the resonance amplitude and broadening of the Fano resonance dip with a

signature of resonance splitting. In the current design, for increased pump fluences, the Fano resonance feature does not show complete switch-off, but rather it shows a signature of resonance splitting that is due to its resonant coupling with the weakly excited phonon modes of the perovskite at room temperature in the lower part of the THz spectrum[37-39] (see the later sections for more discussions). The observed amplitude modulation of Fano resonance is due to gradual shortening of the capacitive split gaps in the TASR structure with increase in photoconductivity of the perovskite layer for increased strengths of the optical excitation pulse. Here, we would like to highlight that this resonant switching behavior happens at ultra-low fluences (< 7 $\mu J/cm^2$) of the optical pump compared with the previous photo-active studies[27,29]. This signifies the ultrasensitive nature of the perovskite based photo-switching of Fano resonances that could provide new directions in designing the ultrasensitive and low threshold photo-active perovskite based metamaterial and plasmonic devices across infrared and far infrared frequencies. We also observe an additional weak resonance splitting at the dipole resonance around 1.1 THz (Fig. 2(a)), in the perovskite-TASR sample for all the pump powers. This resonance splitting occurs due to coupling of the dipolar resonance of the metamaterial with the phonon mode appearing below 10 meV (< 2.4 THz) energies in the perovskite sample. We see that the observed resonance splitting does not show strong dependency on photoconductivity of the perovskite layer. This is due to the low sensitivity nature of the dipolar resonance to the changes in the photoconductivity of the perovskite material.

To further support our claims on active Fano resonance modulation and switching using the solution-processed perovskite layer, we performed extensive numerical simulations using the commercially available CST Microwave studio Frequency solver that solves the Maxwell's equations based on the Finite Integral Techniques. We simulated the frequency response of the TASR metamaterial unit cell, by choosing a lossy aluminum metal with $\sigma_{dc} = 3.56 \times 10^7$ S/m as TASR resonators and quartz ($\varepsilon_r = 3.75$) as a transparent substrate. The simulated transmission spectrum for TASR metamaterial alone (without perovskite layer) is shown by the black curve in Fig. 2(b) that coincides with the corresponding experimental Fano resonance data shown in Fig. 2(a). To simulate the influence of photoconductivity of the perovskite layer on Fano resonance, we placed a 60 nm thick layer of material on the TASR structure by defining the experimentally obtained photoconductivity values of the perovskite sample for the 60 nm thick layered material. Perovskite photoconductivity values were experimentally obtained by measuring the photo-induced transmission change ($-\Delta T/T$) of the

terahertz signal using the OPTP measurements (details are provided in the Supporting Information). Later in the post-processing steps, complex photoconductivity values were extracted by using the thin film optical constants formula (methods are discussed in the Supporting Information). The real part of photoconductivity values at 0.75 THz were chosen to define the optical parameters of the perovskite layer in our numerical simulations for the corresponding pump powers in the measured data. For lower photoconductivity values (< 4976 S/m, pump fluence < 7 $\mu J/cm^2$), numerical results match well with the corresponding experimental data and also shows a complete switch-off of the Fano resonance, where the effects due to phonon-metamaterial resonance coupling are neglected.

In Fig. 3, we provide the numerically simulated electric field distribution at the Fano resonance frequency for the TASR sample with and without the perovskite layer. As seen from Fig. 3(a), *E*-field is concentrated at the gaps of the TASR metamaterial structures. *E*-field is the maximum for the sample without the spin-coated perovskite layer (Fig. 3(a)), whereas for the perovskite coated TASR structure with optical excitation at 7 $\mu J/cm^2$ shows complete annihilation in the strength of *E*-field at the gaps signifying the switching-off of the Fano resonance in the system (Fig. 3(d)). Thus, the perovskite-TASR hybrid system offers very sensitive photo-active switching of the *E*-fields at extremely low optical pump fluences (as low as 7 $\mu J/cm^2$). Hence, the proposed perovskite-TASR metamaterial hybrid system can provide state-of-the-art designs for the ultrasensitive active sensors and can offer huge implications in the future energy efficient photonic devices. Recent studies on the perovskite material have shown its implications as the amplifying medium and have demonstrated the lasing characteristics in these materials[2,7]. Integrating such gain materials with the metamaterial structures such as Fano resonators of high quality factors (Q) can enhance their lasing properties and could help in realizing highly efficient, low threshold and optically active lasing spasers at infrared frequencies that could operate at room temperature.

Furthermore, our studies also reveal that the proposed perovskite-TASR metamaterial hybrid device shows high speed resonant switching behavior. Unlike silicon-based active devices whose switching speeds are in the order of milliseconds, Fano resonances in perovskite-TASR metamaterial device can be switched off and restored within few nanoseconds (~ 20 ns). Figure 4(a) reveals the excitation and relaxation dynamics of the solution processed perovskite layer spun coated on the TASR metamaterial measured using the OPTP setup. Once the sample is photo-excited, its photoconductivity reaches the maximum value near t_p =

6 ps time delay and relaxes back to the steady state within few nanoseconds. For 3.5 μJ/cm^2 of pump fluence, where the recombination dynamics is dominated by the first order recombination process,[18] mainly the trap assisted monomolecular recombination that helps in estimating the decay (life) time of the perovskite sample. We perform a fitting using the rate equation[17-21], $\frac{dx}{dt} = -C^2\varphi^2 k_3 x^3 - C\varphi k_2 x^2 - k_1 x$, where k_1, k_2 and k_3 are the first, second and third order rate constants, C is a constant that depends on the peak number density and φ is the photon-electron conversion efficiency (refer to the supporting information). In Fig. 4 (a), we provide the experimentally measured recombination rates of the sample for the pump fluences of 3.5 μJ/cm^2, 7 μJ/cm^2 and 14 μJ/cm^2 along with the corresponding rate equation fitting. While performing the fitting, the first order rate constant was kept constant, whereas the initial conditions ($\Delta T/T$ at t_p = 6 ps) along with the second and third order rate terms were treated as free parameters. The best fit was achieved for a certain range of k_1 values for which the errors in the other free running parameters were minimum. The fitted parameters are tabulated in the supporting information along with the discussion on recombination dynamics of the bare perovskite sample on quartz without the metamaterial structure. Relaxation life time of the perovskite sample is calculated using the relation, $\tau = k_1^{-1}$ (where $k_1 = 5 \times 10^7$) that is about 20 ns (detailed discussion is provided in the supporting information). Hence, for any pump fluence > 7 μJ/cm^2, Fano resonance can be switched-off instantly with the optical pump illumination (~ 6 ps) and is restored within 20 ns, testifying the high switching speed of the perovskite-metamaterial devices.

Figure 4(b) depicts the terahertz transmission spectra for higher powers of the excitation pulse, where at 0.7 THz, a weak signature of mode coupling is observed. This mode coupling is due to the interaction of the Fano resonance with the optically active phonon mode of the perovskite sample appearing at the Fano resonance frequency. Previous studies on the terahertz characterization of $CH_3NH_3PbI_3$ perovskite have reported [37-39] a weak excitation of the optically active phonon modes in the lower part of the terahertz frequencies at room temperatures. Under the illumination of lower pump fluences (< 7 μJ/cm^2), Fano resonance in the perovskite-TASR sample exhibits strong feature that overshadows the effects of phonon mode on the metamaterial resonances. Hence, no phonon-Fano coupling is observed in the system for the lower pump fluences (< 7 μJ/cm^2). As the Fano resonance feature in the system annihilates with increasing pump fluence, the resonant phonon-Fano coupling becomes prominent, thus resulting in a resonance mode splitting at 0.7 THz for the pump fluences

greater than 14 μJ/cm^2, as seen in Fig. 4(b). On further increase of the pump fluence, the observed resonance splitting shows gradual line-width broadening, thereby indicating the sensitivity of the phonon-Fano coupling to the external optical pump stimulus. Besides the demonstration of ultra sensitive and high speed modulation of Fano resonances, perovskite coated TASR metamaterial design also gives one of the preliminary evidence of resonant phonon-metamaterial mode coupling in the perovskite-metamaterial hybrid system at the terahertz frequencies.

Conclusion

In summary, we have experimentally demonstrated that the solution processed organic-inorganic hybrid lead halide perovskites could be an ideal dynamic material for active photo-switching of the Fano resonance based subwavelength metamaterial devices at terahertz frequencies. The terahertz transmission spectra showed highly sensitive modulation of Fano resonances by optically pumping an extremely thin perovskite film (~ λ/5000) at extremely low fluence of the optical pump beam. We performed numerical simulations to validate the experimental results for the lower photoconductivity values, where the phonon-metamaterial resonance coupling is negligible due to strong Fano resonance feature in the system. For increased pump fluence, where the strength of Fano resonance becomes weaker, the resonance splitting was observed due to the phonon-metamaterial resonance coupling in the system. The observed ultrasensitive switching of the confined *E*-fields can offer new generation active metadevices for sensors, non-linear devices and low threshold lasers. Besides, blending the excellent properties offered by the multifunctional metal halide perovskites and the metamaterials can offer promising steps towards realizing metadevices with enhanced functionalities for nonlinear and lasing applications and for realizing economical and highly efficient active terahertz and optical metamaterial, plasmonic and photonic devices.

References

1. B. R. Sutherland, E. H. Sargent, *Nat. Photon.* **2016,** 10, 295–302.
2. S. A Veldhuis, P. P Boix, N. Yantara, M. Li, T. C. Sum, N. Mathews, S. G Mhaisalkar, *Adv. Mater.*, **2016**, 28, 6804–6834.
3. http://www.nrel.gov/ncpv/index.html, accessed: August 2016.
4. M. A. Green, K. Emery, Y. Hishikawa, W. Warta, E. D. Dunlop, *Progress in Photovoltaics.* **2016**, **24**:3–112015, 137-272, **DOI:** 10.1002/pip.272.
5. Z. K. Tan, R. S. Moghaddam, M. L. Lai, P. Docampo, R. Higler, F. Deschler, M. Price, A. Sadhanala, L. M. Pazos, D. Credgington, F. Hanusch, T. Bein, H. J. Snaith, R. H. Friend, *Nat. Nanotechnol.* **2014**, 9, 687.
6. A. Sadhanala, S. Ahmad, B. Zhao, N. Giesbrecht, P. M. Pearce, F. Deschler, R. L. Z. Hoye, K. C. Gödel, T. Bein, P. Docampo, S. E. Dutton, M. F. L. De Volder, R. H. Friend, *Nano Lett.* **2015**, 15, 6095–6101.
7. G. Xing, N. Mathews, S. S. Lim, N. Yantara, X. Liu, D. Sabba, M. Grätzel, S. Mhaisalkar, T. C. Sum, *Nat. Mater.* **2014**, 13, 476.
8. L. Protesescu, S. Yakunin, M. I. Bodnarchuk, F. Krieg, R. Caputo, C. H. Hendon, R. X. Yang, A. Walsh, M. V. Kovalenko, *Nano Lett.*, **2015**, 15 (6), 3692–3696.
9. T. Leijtens, S. D. Stranks, G. E. Eperon, R. Lindblad, E. M. J. Johansson, I. J. McPherson, H. Rensmo, J. M. Ball, M. M. Lee, H. J. Snaith, *ACS Nano*, **2014**, 8 (7), 7147–7155.
10. S. D. Stranks, G. E. Eperon, G. Grancini, C. Menelaou, M. J. P. Alcocer, T. Leijtens, L. M. Herz, A. Petrozza, H. J. Snaith, *Science,* **2013***,* 342, 341–344.
11. G. Xing, N. Mathews, S. Sun, S. S. Lim, Y. M. Lam, M. Grätzel, S. Mhaisalkar, T. C. Sum, *Science* **2013**, 342, 344–347.
12. W. Nie, H. Tsai, R. Asadpour, J-C. Blancon, A. J Neukirch, G. Gupta, J. J. Crochet, M. Chhowalla, S. Tretiak, M. A. Alam, H-L Wang, A. D. Mohite, *Science,* **2015***,* 347, 522–525.
13. W. S. Yang, J. H. Noh, N. J. Jeon, Y. C. Kim, S. Ryu, J. Seo, S. I. Seok, *Science* **2015**, 348, 1234–1237.
14. H. Zhou, Q. Chen, G. Li, S. Luo, T-b. Song, H-S. Duan, Z. ng, J. You, Y. Liu, Y. Yang, *Science* **2014**, 345,542–546.

15. M. Saliba, S. M. Wood, J. B. Patel, P. K. Nayak, J. Huang, J. A. A-Webber, B. Wenger, S. D. Stranks, M. T. Hörantner, J. T-W. Wang, R. J. Nicholas, L. M. Herz, M. B. Johnston, S. M. Morris, H. J. Snaith, M. K. Riede, *Adv. Mater.* **2016**, 28, 923–929.
16. R. Dhanker, A. N. Brigeman, A. V. Larsen, R. J. Stewart, J. B. Asbury and N. C. Giebink, *Appl. Phys. Lett*. **2014**, 105, 151112.
17. C. Wehrenfennig, G. E. Eperon, M. B. Johnston, H. J. Snaith, L. M. Herz, *Adv. Mater*. **2014**, 26, 1584–1589.
18. L. M. Herz, *Annu. Rev. Phys. Chem.* **2016**, 67, 65–89.
19. M. B. Johnston and L. M. Herz*, Acc. Chem. Res.,* **2016***,* 49, 146–154.
20. R. L. Milot, G. E. Eperon, H. J. Snaith, M. B. Johnston, L. M. Herz, *Adv. Funct. Mater*. **2015**, 25, 6218-6227.
21. C. L. Vorakiat, T. Salim, J. Kadro, M-T. Khuc, R. Haselsberger, L. Cheng, H. Xia, G. G. Gurzadyan, H. Su, Y. M. Lam, R. A. Marcus, M-E. M-Beyerle, E. E. M. Chia, *Nat. Commun*. **2015**, 6, 7903.
22. B. Gholipour, G. Adamo, D. Cortecchia, H. N. S. Krishnamoorthy, M. D. Birowosuto, N. I. Zheludev, C. Soci, *Adv. Mater*. **2017**, 29, 1604268.
23. J. B. Pendry, A. J. Holden, D. J. Robbins, and W. J. Stewart, *IEEE Trans. Microwave Theory Tech*. **1999**, 47, 2075.
24. D. R. Smith, J. B. Pendry, M. C. K. Wiltshire, *Science* **2005**, 305, 788-792.
25. J. B. Pendry, *Phys. Rev. Lett*. **2000**, 85, 3966.
26. T. J. Yen, W. J. Padilla, N. Fang, D. C. Vier, D. R. Smith, J. B. Pendry, D. N.Basov, and X. Zhang, *Science* **2004**, 303(5663), 1494-1496.
27. W. J. Padilla, A. J. Taylor, C. Highstrete, M. Lee, R. D. Averitt, *Phys. Rev. Lett*. **2006**, **96**, 107401.
28. H-T. Chen, J. F. O'Hara, A. K. Azad, A. J. Taylor, R. D. Averitt, D. B. Shrekenhamer, and W. J. Padilla, *Nat. Photon*. **2008**, 2, 295–298.
29. M. Manjappa, Y. K. Srivastava, L. Cong, I. Al-Naib, and R. Singh, *Adv. Mater.* **2017**, 29 (3), 1603355. **DOI** 10.1002/adma.201603355.
30. H. Tao, A. C. Strikwerda, K. Fan, W. J. Padilla, X. Zhang, R. Averitt, *Phys. Rev. Lett*. **2009**, 103, 147401.
31. P Pitchappa, M Manjappa, CP Ho, R Singh, N Singh, C Lee, *Adv. Opt. Mater.* **2016**, 4, 541–547.
32. Q. Li, Z. Tian, X. Zhang, R. Singh, L. Du, J. Gu, J. Han, W. Zhang, *Nat. Commun*. **2015**, 6, 7082.

33. R. Singh, I. A. I. Al-Naib, M. Koch, W. Zhang, *Optics Express,* **2011**, 19 (7), 6312-6319.
34. B. luk'yanchuk, N. I. Zheludev, S. A. Maier, N. J. Halas, P. Nordlander, H. Giessen, C. T. Chong, *Nat. Mater.* **2010**, 9, 707-715.
35. N. I. Zheludev, S. L. Prosvirnin, N. Papasimakis, and V. A. Fedotov, *Nat. Photon.* **2008**, 2, 351-354.
36. S. S. Lim, W. K. Chong, A.Solanki, H. A. Dewi, S. Mhaisalkar, N. Mathews, T. C. Sum, *Phys. Chem. Chem. Phys.* (**2016**) **DOI:** 10.1039/C6CP02640K.
37. Chan La-o-vorakiat, Huanxin Xia, Jeannette Kadro, Teddy Salim, Daming Zhao, Towfiq Ahmed, Yeng Ming Lam, Jian-Xin Zhu, Rudolph A. Marcus, Maria-Elisabeth Michel-Beyerle, and Elbert E. M. Chia, *J. Phys. Chem. Lett.* **2016**, 7, 1−6.
38. M. Bokdam, T. Sander, A. Stroppa, S. Picozzi, D. D. Sarma, C. Franchini, G. Kresse, *Scientific Reports* **2016**, 6, 28618.
39. C. La-o-vorakiat, L. Cheng, T. Salim, R. A. Marcus, M. E. M. Beyerle, Y. M. Lam, and E. E. M. Chia. *Appl. Phys. Lett.* **2017**, 110, 123901.

Supporting Information
Supporting Information is available online from the Wiley Online Library or from the author.

Acknowledgements

The authors acknowledge research funding support from NTU startup Grant Nos. M4081282, M4080514 and, Singapore Ministry of Education Academic Research Fund Grant Nos. RG184/14, M4011362, M4011534, MOE2011-T3-1-005, MOE2014-T2-1-044, MOE2015-T2-2-015 and MOE2015-T2-2-103.

R. S. conceived the idea. M. M., Y. K. S, and R. S. designed the experiments. M. M performed all the OPTP measurements and analysis. Y. K. S fabricated the metamaterial devices and performed the numerical simulations. A. S. spun coated the perovskite film on metamaterial device and optimized the process. A. S and Y. K. S performed the AFM and XRD characterization of the perovskite film on metamaterial. A. K. performed extraction of photo-conductivity and rate constants. R. S. and T. C. S supervised the overall work. All the authors analyzed and discussed the results. M. M. and R. S. wrote the manuscript with inputs from all the authors.

Figures

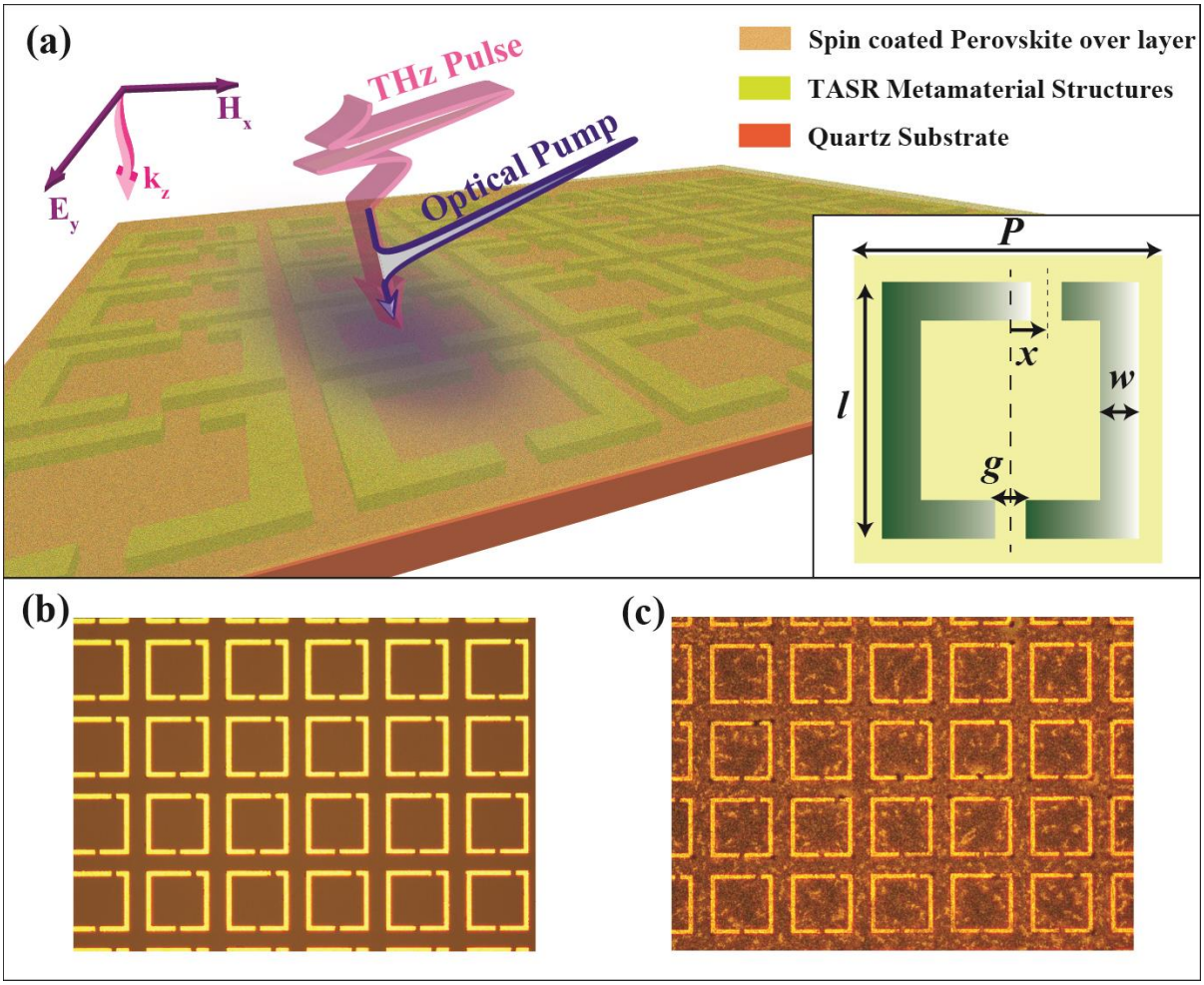

Figure 1: **(a)** Graphical representation proposed perovskite-metamaterial device consisting of a hybrid lead halide perovskite film spin coated terahertz asymmetric split ring (TASR) metamaterial structure. The OPTP characterization is performed with the normal illumination of the optical pump pulse (400 nm) and the terahertz probe pulse. The inset diagram shows the unit cell of the TASR metamaterial structure with the structural dimensions; Periodicity, P : 75 μm; length, l : 60 μm; width, w : 6 μm; gap, g : 3 μm; and asymmetry, x : 15 μm. Optical microscope images of the fabricated planar TASR metamaterial structure **(b)** without the perovskite layer and **(c)** with the 60 nm thin layer of spin-coated perovskite film showing uniform deposition.

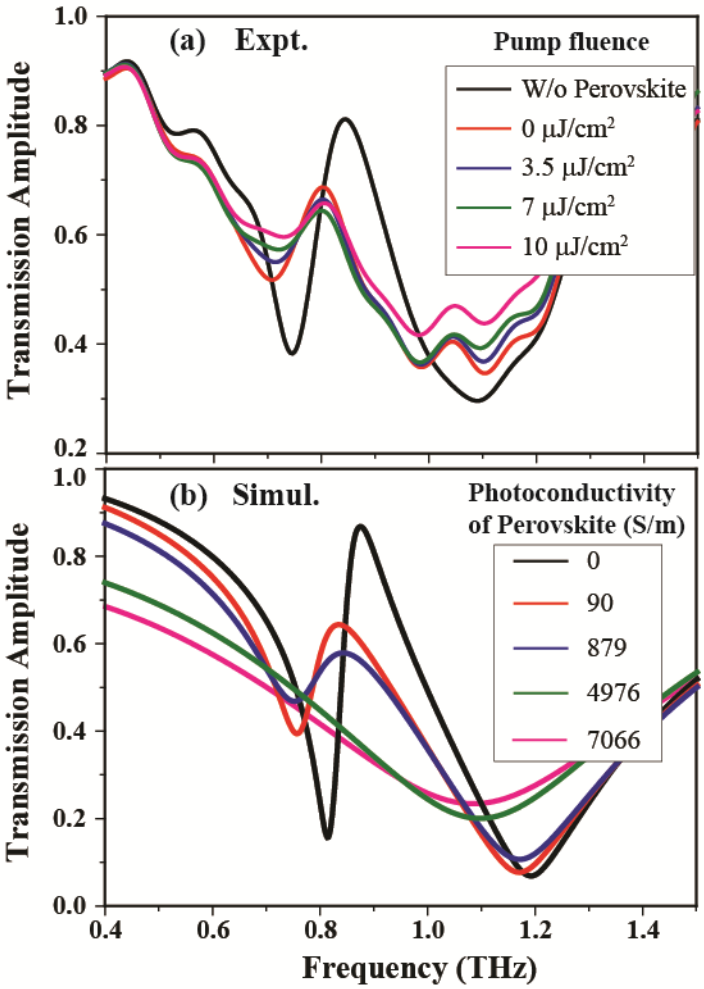

Figure 2. **(a)** Measured terahertz transmission spectra for the TASR metamaterial structure showing the modulation of Fano resonance without and with the spin coated perovskite layer for varying powers of the optical photo-excitation pulse extracted using OPTP measurements. **(b)** Corresponding numerically simulated transmission spectra by changing the photoconductivity of perovskite layer deposited on the TASR metamaterial structure. The photoconductivity values of perovskite in (b) are proportional to the optical pump fluences shown in (a) and the correspondence is shown by same color plots in (a) and (b).

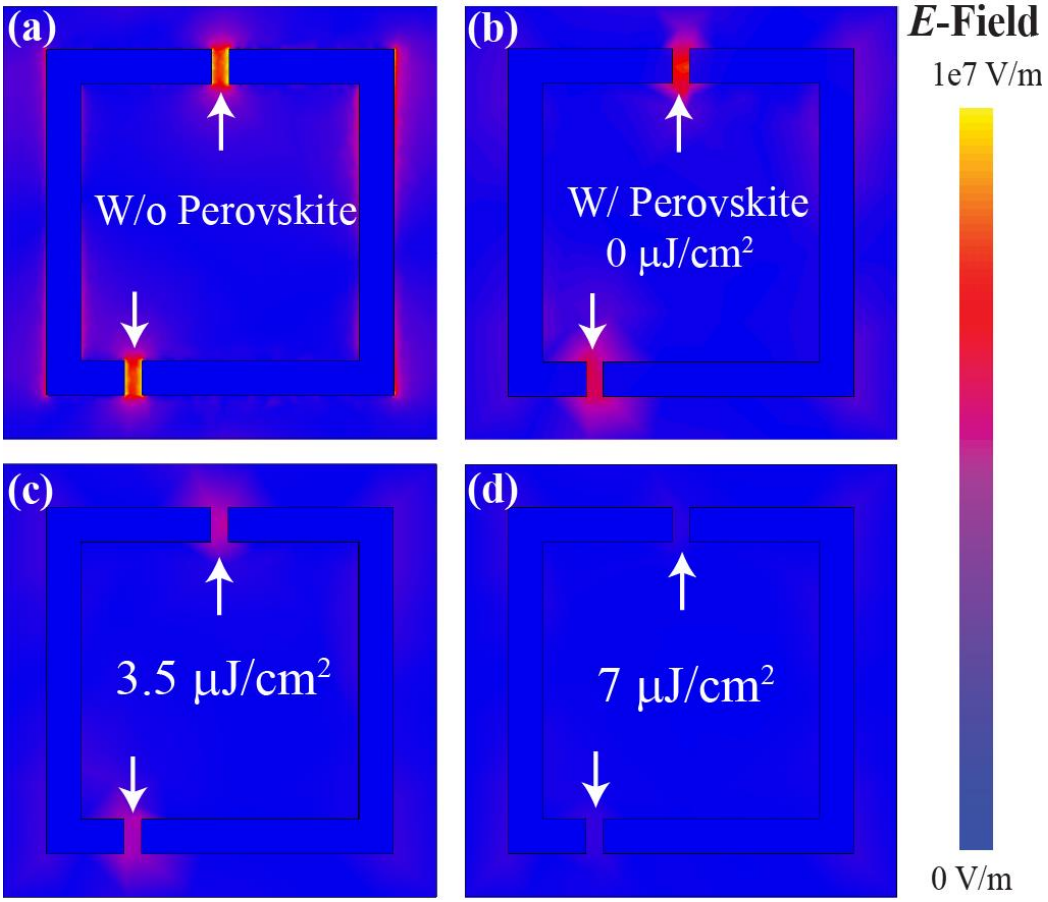

Figure 3. Numerically calculated *E*-field distributions in the split gap of the TASR metamaterial structure extracted at the Fano resonance frequency. For the sample **(a)** without the perovskite layer shows the strong *E*-field confinement at the gaps (shown by the arrows) and **(b)** with the perovskite layer and without the photo-excitation, the *E*-fields show slight decrease. For the photo-excited sample with pump powers of **(c)** 1 mW, *E*-field shows further reduction and for **(d)** 2 mW, it almost disappears.

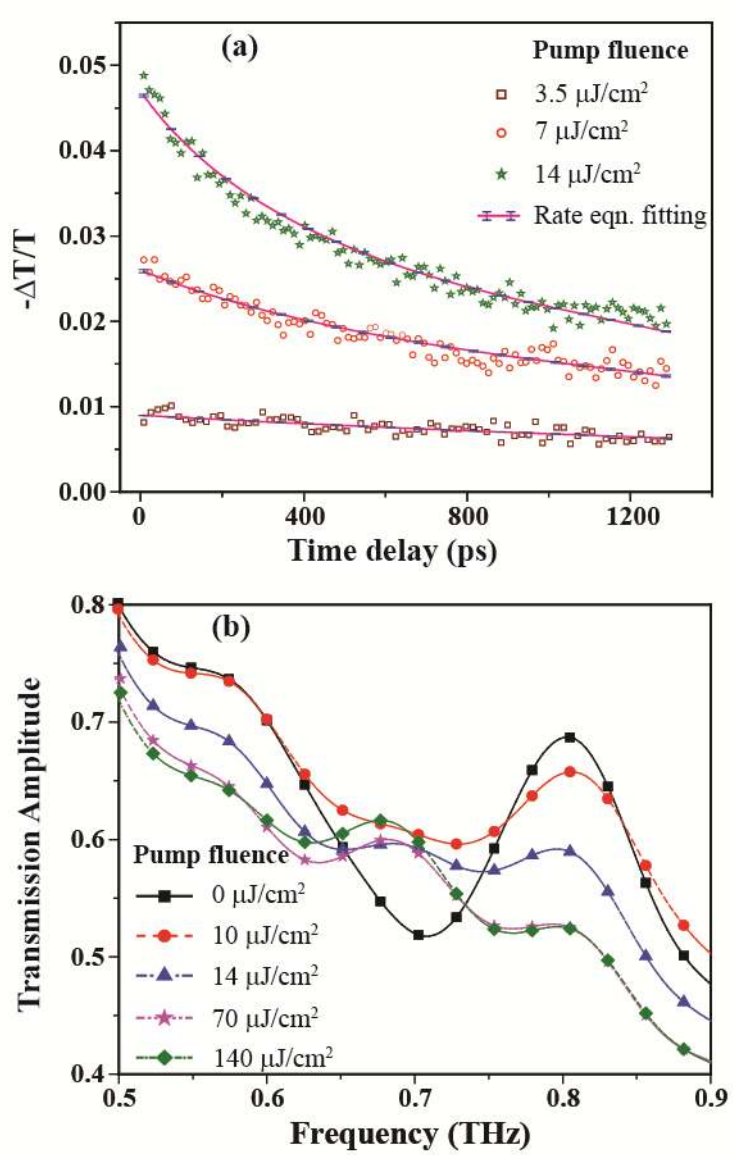

Figure 4. **(a)** Depicts the excitation dynamics of the solution processed perovskite ($CH_3NH_3PbI_3$) sample spin coated on the TASR (Fano) resonators for various pump fluences performed by using the OPTP measurements. Solid magenta line depicts the fitting of the recombination dynamics for the corresponding pump fluences using the described rate equation (Eqn. 1). The uncertainties are calculated using the standard deviation method. **(b)** Experimentally measured transmission spectra depicting the mode splitting of the resonance curves at 0.7 THz for higher optical pump fluences due to the resonant phonon-Fano resonance interaction. In the legend, 0 $\mu J/cm^2$ corresponds to absence of photo-excitation of the perovskite sample, whereas 140 $\mu J/cm^2$ represents the stronger photo-excitation of the perovskite sample.

Supporting Information

for *Adv. Mater.*, DOI: 10.1002/adma.((.....))

Hybrid Lead Halide Perovskites for Ultrasensitive Photo-Active Switching in Terahertz Metamaterial Devices

Manukumara Manjappa, Yogesh Kumar Srivastava, Ankur Solanki, Abhishek Kumar, Tze Chien Sum, and Ranjan Singh.*

* Corresponding author: *ranjans@ntu.edu.sg*.

Sample Preparation

The metamaterial sample consisting of 200 nm thick aluminum resonators was fabricated using the standard photolithography technique on a z-cut quartz substrate of thickness 1 mm. Quartz substrate was cleaned using acetone and IPA. After drying the substrate at 100 °C for 10 mins on a hot plate, a positive photoresist of thickness 1.5 µm was coated on it. A positive mask that consists of resonators design was aligned on the photoresist on quartz substrate and was exposed to UV light after prebaking at 105° C. Later, it was soaked in a developer solution to develop the pattern. After patterning, 200 nm thick aluminum was deposited using thermal evaporation method and as a final step, it was soaked in acetone solution to liftoff the undesired aluminum to get the final metallic metamaterial structure, as shown by the optical microscope image in Fig. 1(b) of the main article.

On the other hand, perovskite ($CH_3NH_3PbI_3$) solution was prepared by using a standard and adequate process based on magnetic stirring, where 78.3 mg/ml lead(II) iodide (Acros Organics PbI_2) and 27.0 mg/ml methylammonium iodide (DyeSol CH_3NH_3I) was dissolved in N,N-Dimethylformamide (Sigma Aldrich DMF) in a N_2-filled glovebox to obtain a clear yellow 10 wt. % methylammonium lead iodide ($CH_3NH_3PbI_3$) solution. Neat perovskite films were obtained on the metamaterial structure by single-step deposition by spin-coating the heated perovskite solution (70 ^oC) onto a cleaned metamaterial sample at 4000 RPM for 30 seconds. This method of depositing the perovskite on the photonic device can be compatible on much more complex metamaterial structures. For example, the solution processed

perovskite can be spin coated onto the metamaterial patterned on the flexible substrates, multilayered metamaterial structures, hyperbolic metamaterials and various other photonic devices. The spin coating of perovskite also depends on the choice of the substrates such as silicon, indium tin oxide coated glass, polyethylene terephthalate (PET) etc. It is also applicable to scale-up applications using screen printing and doctor blade technique.

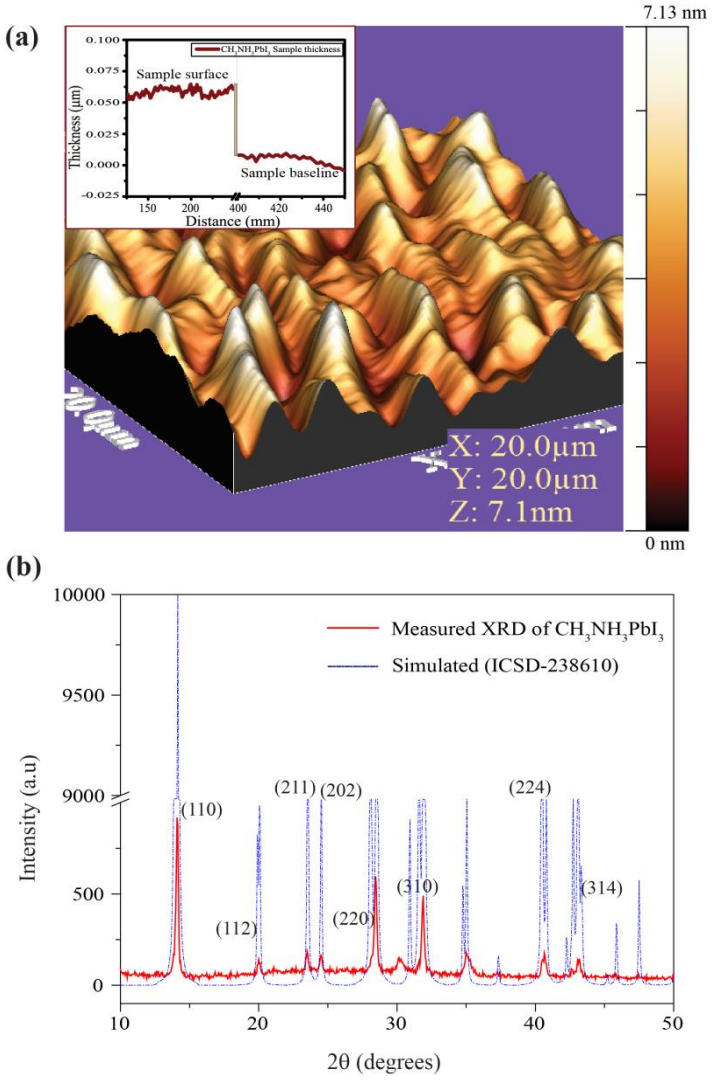

Figure S1. (a) 3D Atomic-force microscopy (AFM) image of the solution processed $CH_3NH_3PbI_3$ perovskite spin coated on the quartz substrate. The inset graph depicts the profilometry data, which shows the uniform thickness (60 nm) of the spun-coated perovskite layer on the TASR metamaterial structure. **(b)** Measured X-ray diffraction (XRD) spectra of the $CH_3NH_3PbI_3$ perovskite sample overlapped with the simulated XRD spectrum extracted from the literature (Source: ICSD-238610).

AFM image of the spin-coated perovskite film is shown in the Fig. S1(a), which are obtained using the Asylum Research MFP-3D AFM system in the tapping mode. The peak to peak height and the RMS roughness value of the sample is measured to be about 7.13 nm and 1.09 nm, respectively, which is negligible compared to the thickness (60 nm) of the perovskite thin

film. We carried out surface profilometry measurements to measure the thickness and surface uniformity of the spun-coated perovskite sample. As shown in the inset of Fig. S1(a), the profilometry data shows a uniform thickness of 60 nm over layer perovskite sample. We also carried out X-ray diffraction (XRD) measurements on the spin-coated perovskite sample and the corresponding spectrum in comparison to the theoretical predictions (from the literature, ICSD-238610) is shown in Fig. S1(b). The measured XRD spectrum shows most of the dominant $CH_3NH_3PbI_3$ diffraction peaks. A good agreement of the measured XRD data with the literature values confirms the purity of the prepared perovskite sample spin coated on the TASR metamaterial structure.

Optical pump-Terahertz probe Measurements

The terahertz transmission measurements were carried out using Optical-pump-Terahertz-probe setup that is based on ZnTe nonlinear THz generation and detection. Optical laser beam used for the generation of terahertz and for photo-excitation of the perovskite sample has a pulse width of ~ 100 fs, energy of 4 mJ/pulse at 800 nm with a 1 kHz repetition rate. The beam was split into two parts with one being used for pumping the ZnTe crystal for THz generation-detection and the other part of the beam was frequency doubled (400 nm, 3.1 eV) using a BBO crystal for optical excitation of perovskite. The photo-excitation pulse has higher photon energy than the band gap of the $CH_3NH_3PbI_3$ perovskite sample, which is about 1.6 eV (770 nm). The optical pump beam has a beam diameter of approx. 6 mm, which is much larger than the focused terahertz beam spot size of nearly 3 mm at the sample position, providing uniform photo-excitation over the perovskite film. The time delay between optical-pump and terahertz probe pulses was controlled by using a translational stage and the delay is set to about 6 ps, where the photo-excited signal is the maximum. At this maximum pump signal, the terahertz scan was performed on the sample and the reference substrate and later in the post processing steps the spectrum through the sample ($E_S(\omega)$) is normalized to the reference substrate transmission spectra ($E_R(\omega)$) using the relation $|T(\omega)| = |E_S(\omega)|/|E_R(\omega)|$, the same is plotted in Figs. 2(a) and 4(b) of the main article.

Photoconductivity measurements

The differential transmission ($-\Delta T/T$) data of the terahertz pulse through the optically pumped perovskite thin film is used to extract the photoconductivity of the perovskite sample for various pump powers. For a thin film sample on a nonconducting, semi-infinite and non-absorbing substrate, the complex transmission is given by[1],

$$T(\omega, t_p) = \frac{\tilde{T}_p(\omega,t_p)}{\tilde{T}_{Ref}(\omega)} = \frac{n+1}{n+1+Z_0\Delta\tilde{\sigma}(\omega,t_p)d} \quad (1)$$

Where, $\tilde{T}_P(\omega, t_p) = \tilde{T}_{Ref}(\omega) + \Delta\tilde{T}(\omega, t_p)$ is the THz pulse with photo-excitation, Z_0 = 377 Ω is the impedance of the free space, d is the thickness of sample (d<< λ) and n is the refractive index of substrate at THz region. The complex photoconductivity ($\Delta\tilde{\sigma}$) of the thin film perovskite sample can be extracted numerically by solving the Eqn. S1 as below.

$$\Delta\tilde{\sigma}(\omega, t_p) = \frac{n+1}{Z_0 d}\left[\frac{1-T(\omega,t_p)}{T(\omega,t_p)}\right] \quad (2)$$

The extracted real part of the photoconductivity spectra for different pump fluences are plotted in Fig. S2. By increasing incident pump fluence, the number of photo-exited carriers in the perovskite sample increases. As a result, the photoconductivity of the perovskite increases with the increasing pump fluence. The conductivity value at 0.75 THz (resonance frequency of the Fano absorption dip) is chosen as the pump induced material parameter in our numerical simulations.

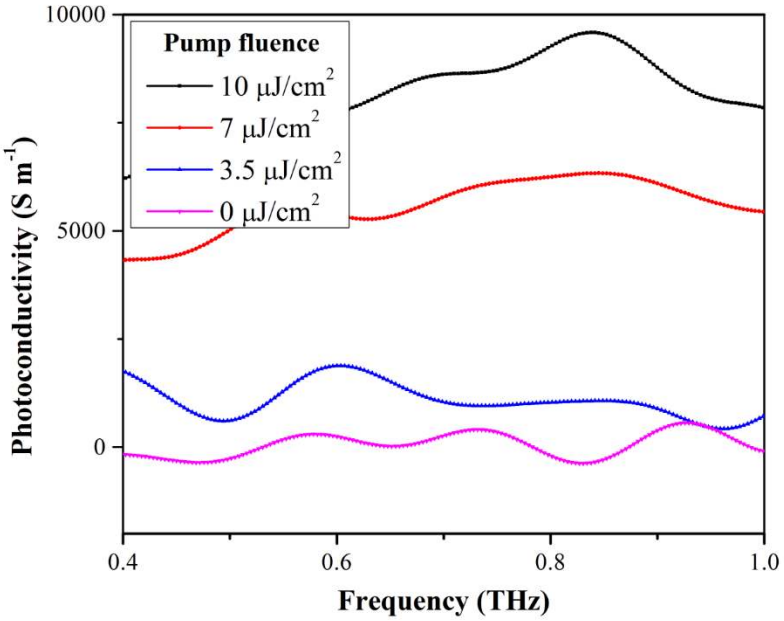

Figure S2. Real part of the photoconductivity spectrum ($\Delta\tilde{\sigma}_R$) extracted using Equation S2 for the $CH_3NH_3PbI_3$ perovskite thin film on a z-cut quartz substrate using Optical pump-THz probe (OPTP) measurements. The legends represent the fluence of the optical excitation pump pulse.

Recombination life time calculations

The recombination dynamics of the perovskite sample spun-coated on the metamaterial sample is probed using the OPTP measurements, as shown in the Fig. 4(a) of the main article. The recombination mechanisms and dynamics of free charge carrier density plays a

fundamental role in the functioning of semiconductors materials that elucidates the non-resonant and resonant non equilibrium dynamics in the system. The rate equations are fitted to the recombination dynamics to extract the relaxation life time and other higher order recombination processes. The rate equation is described by the following expression[2],

$$\frac{dn}{dt} = -k_1 n - k_2 n^2 - k_3 n^3 . \qquad (3)$$

Where, k_1 is the rate constant related with monomolecular recombination (trap-assisted recombination), k_2 is the bi-molecular charge carrier recombination rate and k_3 is the rate constant that describes Auger recombination (many body recombination).

To study these dynamics, we analyzed differential change in the THz transmission $\frac{-\Delta T}{T}(t)$ for different pump power of the incident pump beam, because this experimentally observed THz transient is proportional to the free carrier density and it can be written as, $n(t) = \varphi\, C\, x(t)$, where, $C = {n_0}/{x(0)}$ is the proportionality constant which depends on immediate THz response $x(0) = -\frac{\Delta T}{T}(0)$.

The maximum absorbed photon density is given by, $n_0 = \frac{E\lambda\alpha(\lambda)}{hcA_{eff}}(1 - R_{pump})$, where α is the absorption coefficient of the sample at the excitation wavelength (λ = 400nm in our case). After substituting all the parameters to the Eqn. S3 the rate equation becomes,

$$\frac{dx}{dt} = -C^2\varphi^2 k_3 x^3 - C\varphi k_2 x^2 - k_1 x \qquad (4)$$

Hence, fitting the recombination dynamics with the rate equation (Eqn. S4) gives the information about the different orders of recombination. We have fitted the numerical solutions of above differential equation (Eqn. S4) to the observed THz transients for various pump fluences to extract rate constants of different orders. Since at the lower fluence (3.5 μJ/cm^2) the recombination dynamics is governed by first order rate equation, so fitting the lower power THz transients gives the information about recombination lifetime $(k_1)^{-1}$ of the sample. The fitting is given for the 3.5 μJ/cm^2, 7 μJ/cm^2 and 14 μJ/cm^2 pump dynamics in the Fig. 4(a) of the main article, where the calculated recombination life time for the perovskite sample (with metamaterial) is in the range of 3 ns to 20 ns for the different pump fluences, as shown in the below **Table S1**. However, THz transients for all the fluences are fitted by using the same differential equation (Eqn. S4). The rate equation fitting of THz transients for different fluences (without metamaterial structure) is shown in Fig. S3 with the uncertainty in

the fitting values of k_1, k_2 and k_3 as given in the **Table S2**. The uncertainties in the rate constants for a perticular fluenece are calculated using the standard deviation method by fitting the measured relaxation dynamics data for a range of k_1 values, for which the errors in the values of k_2 and k_3 are minimum. Here, we also would like to emphasize on the fact that the transient THz measurements can only give near estimation on the life times but will not determine the exact life times of the sample, which is only determined by the time resolved photoluminescence spectroscopy [Ref. 18 of manuscript] and hence the observed large uncertainties (range) in the life time values of the perovskite and are given in the table below (Table S1 and Table S2).

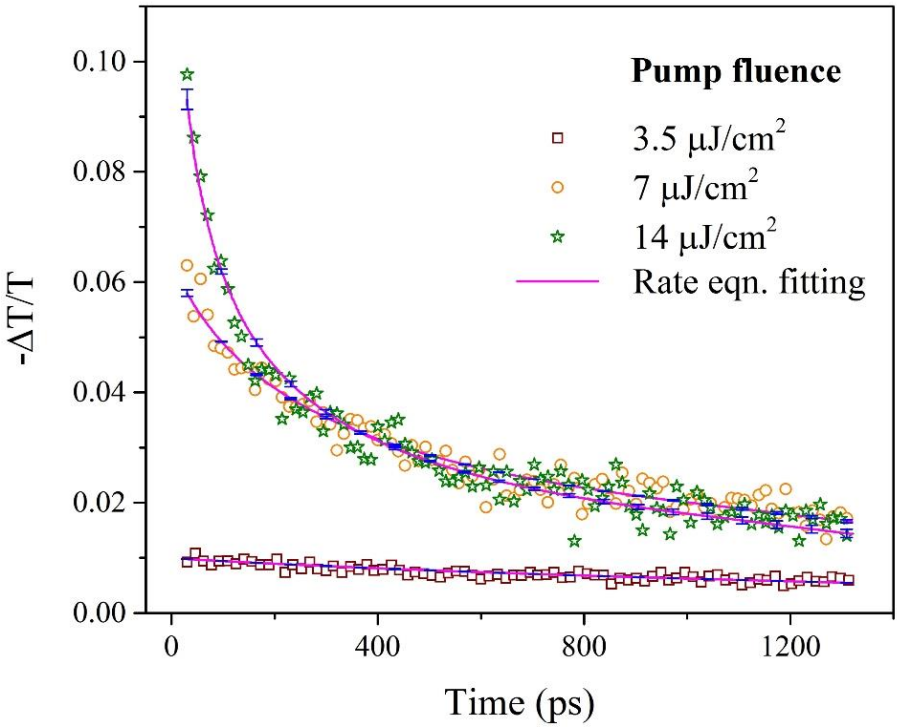

Figure S3. Experimentally measured recombination dynamics for the perovskite sample (without metamaterial) using the OPTP setup. The uncertainties are calculated using the standard deviation method.

Pump fluences	**Approx. Life time (k_1^{-1})**	**k_1 (range)**	**Cφk_2**	**$C^2\varphi^2 k_3$**
3.5 μJ/cm²	4 ns to 20 ns	5e7 to 2.5e8	2.56e10 +/- 9.53e9	-------
7 μJ/cm²	5 ns to 20 ns	5e7 to 2e8	1e10 +/- 2.9e9	7.8 e11 +/- 1.5e11
14 μJ/cm²	11 ns to 20 ns	5e7 to 9e7	1e10 +/- 1.12e9	4.8e11 +/- 3.7e10

Table S1. Fitted parameters (along with the uncertainties in their fitted values) for the recombination dynamics of the perovskite sample spin coated on a metamaterial structure.

Pump fluences	Approx. Life time (k_1^{-1})	k_1 (range)	$C\varphi k_2$	$C^2\varphi^2 k_3$
3.5 μJ/cm²	3 ns to 14 ns	7e7 to 3e8	4.28e10 +/- 1.05e10	-------
7 μJ/cm²	5 ns to 14 ns	7e7 to 2e8	1e10 +/- 1.49e9	7.17e11 +/- 4.69e10
14 μJ/cm²	3 ns to 14 ns	7e7 to 3e8	1e10 +/- 1.31e9	1e12 +/- 3.5e10

Table S2. Fitted parameters along with their uncertainties for the recombination dynamics of the perovskite sample *without* the metamaterial structure.

Numerical Simulations

Numerical calculations were performed using commercially available simulation software; Computer Software Technology (CST) Microwave studio Frequency Solver which is based on Finite Integral Techniques. The aluminium metal of thickness 200 nm with DC conductivity, $\sigma_{DC} = 3.56 \times 10^7$ S/m was used to model metallic terahertz asymmetric ring resonator (TASR) and the quartz of thickness 1 mm with permittivity of 3.75 was chosen as the transparent substrate. On the top of the metallic structure 60 nm thick layer of material was placed and its optical property was defined by experimentally measured photoconductivity of the perovskite layer at different excitation pump powers. An infinite array of the above designed structure is considered during simulations using unit cell boundary conditions in planar directions. The terahertz wave with the electric component of the field polarized perpendicular to the gap of TASR is normally incident on the designed metamaterial structure. The transmission response for varying photoconductivity of the perovskite layer is shown in Fig. 2(b) of the main article.

Supporting References

1. P. U.Jepsen, D. G. Cooke, M. Koch, Terahertz spectroscopy and imaging – Modern techniques and applications. *Laser Photonics Rev*. **2011**, 5(1), 124–166.
2. C.Wehrenfennig, M. Liu, H. J. Snaith, M. B. Johnston, L. M. Herz, Charge-carrier dynamics in vapour-deposited films of the organolead halide perovskite $CH_3NH_3PbI_{3-x}Cl_x$. *Energy Environ. Sci.,* **2014**, **7**, 2269.